

## Article

# Research on the Formation, Microstructure, and Properties of 304 Stainless Steel AC-DC Hybrid TIG Welding

Ying Ye, Bairu Yang, Yonghui Yang, Zihan Pan, Chao Chen \* and Xinlong Zhang \*

College of Mechanical and Electrical Engineering, Northeast Forestry University, Harbin 150040, China

\* Correspondence: chaochenaw@126.com (C.C.); zhangxinlong2009@nefu.edu.cn (X.Z.)

**Abstract:** In this work, a new welding method, AC-DC hybrid TIG welding, is used to weld 304 stainless steel. Research on the formation, microstructure, and properties of 304 stainless-steel welded joints are studied by using optical microscope and microhardness. The results show that the weld with AC/DC hybrid welding is a fish-scale pattern, and the density of the fish-scale pattern increases with the increase of AC proportion. Both the weld penetration and the ratio of weld penetration to weld width are the highest when AC accounts for 30%. At this point, the weld penetration is 0.83 mm larger than DC mode, an increase of 93.26%, and the ratio of weld penetration to weld width is 1.6, which is 76.19% higher than DC mode. When the proportion of AC is increased, the microstructure of the weld is equiaxed or columnar, and the microstructure of the heat-affected zone is ferrite in the form of lath. The hardness of the weld is greater than that of the base metal, and the hardness of the heat-affected zone is the lowest. The microhardness distribution of the weld with AC 50% is the most uniform. When AC accounts for 20% and 30%, the average weld hardness is the highest, which are 196.7 HV and 198.1 HV, respectively.

**Keywords:** TIG welding; AC-DC hybrid; forming; microstructure



**Citation:** Ye, Y.; Yang, B.; Yang, Y.; Pan, Z.; Chen, C.; Zhang, X. Research on the Formation, Microstructure, and Properties of 304 Stainless Steel AC-DC Hybrid TIG Welding. *Metals* **2023**, *13*, 1127. <https://doi.org/10.3390/met13061127>

Academic Editor: Alfonso Paoletti

Received: 22 March 2023

Revised: 7 June 2023

Accepted: 14 June 2023

Published: 16 June 2023



**Copyright:** © 2023 by the authors. Licensee MDPI, Basel, Switzerland. This article is an open access article distributed under the terms and conditions of the Creative Commons Attribution (CC BY) license (<https://creativecommons.org/licenses/by/4.0/>).

## 1. Introduction

Stainless steel has corrosion resistance, mechanical properties, good durability, and easy forming and processing and is widely used in petroleum, chemical, machinery, nuclear power, building, and other fields [1–4]. At present, the TIG welding of stainless steel is being optimized to continuously improve the quality of welded joints [5–8]. The production austenitic stainless-steel mode and the existing welding problems are difficult to meet the huge market demand, such as common argon arc welding, slow welding speed, and low production efficiency. Tungsten inert gas welding (TIG) is characterized by excessive welding heat input, coarse weld grain, and high corrosion resistance [9,10]. Laser welding, expensive equipment, complex technology, and the welding process are prone to pulsation and clearance changes, which affect the quality of weld forming [11,12]. Therefore, it is of great significance to select a high efficiency, stable, and good quality welding technique for rapid production of austenitic stainless-steel tubes [13,14].

The appearance of arc composite welding improves the quality of argon tungsten inert gas welding to a great extent. It is usually compounded by changing the current output mode and adding energy fields [15–17]. Cong Baoqiang et al. [18,19] added the ultrasound square wave current to the TIG power supply and developed a new TIG welding method, namely, ultra-fast transformation of composite pulse with variable polarity TIG welding. In addition, in recent years, in order to improve the quality of stainless-steel welded joints, many stainless-steel welding technologies have been studied, such as resistance upset welding (UW) [20], laser-arc hybrid welding [21], and tungsten inert gas arc welding (TIG) [22]. Among them, TIG welding using inert gas (He or Ar gas) is a method to prevent oxidation and nitriding of materials and to combine non-ferrous metals. This method has the advantage of obtaining a smooth weld surface. TIG welding is one of the best welding methods [22].

At present, the TIG welding of stainless steel is being optimized to continuously improve the quality of welded joints. A number of studies have found that the electrical waveform has a great influence on the performance of TIG welded joints. The welding quality and arc performance can be improved by adjusting the current waveform of the power supply. Mingxuan Yang et al. showed that the arc characteristics under pulsed current affect the molten pool fluid state which affects the microstructure and mechanical properties of welded joints. Additionally, the pulse frequency can optimize the mechanical properties of welded joints, such as toughness and ductility [23]. Wang, Y. J. et al. showed that the high frequency pulse can produce an ultrasonic effect on arc and molten pool, and the amplitude of modulated pulse current is the main factor affecting ultrasonic sound pressure and power [24]. Manti, R. et al. found that pulsed TIG welding is superior to traditional argon arc welding in some aspects. Pulse parameters can affect the grain structure of the heat affected zone, fusion line, and weld metal [25].

From the literature, it can be seen that there is relatively little research on the different welding input electrical signals of stainless steel at present. A new type of TIG welding signal waveform is proposed, that is, AC/DC mixed waveform 304 stainless steel AC-DC mixed TIG welding. The effects of different AC ratios on the weld formation, mechanical properties, and microstructure of welded joints are systematically studied.

## 2. Experimental Materials and Experimental Methods

### 2.1. Experimental Materials

The variety of 304 stainless steel is used as the base metal in the experiment, and its dimensions are 100 mm × 100 mm × 2 mm. The chemical composition obtained from the literature is shown in Table 1. According to tensile experiments, the mechanical properties of 304 stainless steel are as follows: tensile strength = 684.1 MPa, elongation = 56.43%, and yield point = 205 MPa. Wenjun Zhang et al. [4] reported that the microstructure of 304 stainless steel is strain-induced martensite, austenite about 56 μm in size, and a small amount of twin.

**Table 1.** Chemical composition of 304 stainless steel (mass fraction, %).

C	Mn	P	S	Ni	Cr
0.06	1.84	0.02	0.02	8.23	18.5

### 2.2. Experimental Method

The experiments were adopted by TIG self-melting welding, and the material is 304 stainless steel. After comparing several sets of experiments in the pre-experiment, the best experimental parameters are obtained. Relevant experimental parameters are welding current (80 A), height between the surface of the test plate and the tip of the tungsten pole (2 mm), diameter of the tungsten pole (2.4 mm), and welding speed (4 mm/s). The shielding gas used in the welding process of this experiment is argon, and the flow rate is 15 L/min. The experimental equipment diagram is shown in Figure 1a. The model of the welder is MasterTig335AC/DC. The left side of the equipment diagram shows the enlarged welding part.

There are eleven groups of experiments that are conducted using self-fusion welding, and now from the aspects of weld molding, microstructure, and performance, the differences in welding under different AC proportion conditions are studied, as shown in Table 2. The experimental welding mode can be divided into three types: DC mode, AC mode, and AC/DC hybrid mode. Among them, the size and direction of direct current does not change; the size and direction of alternating current changes periodically, and AC and DC mixing means that alternating current and direct current appear periodically. This is shown in Figure 1b.

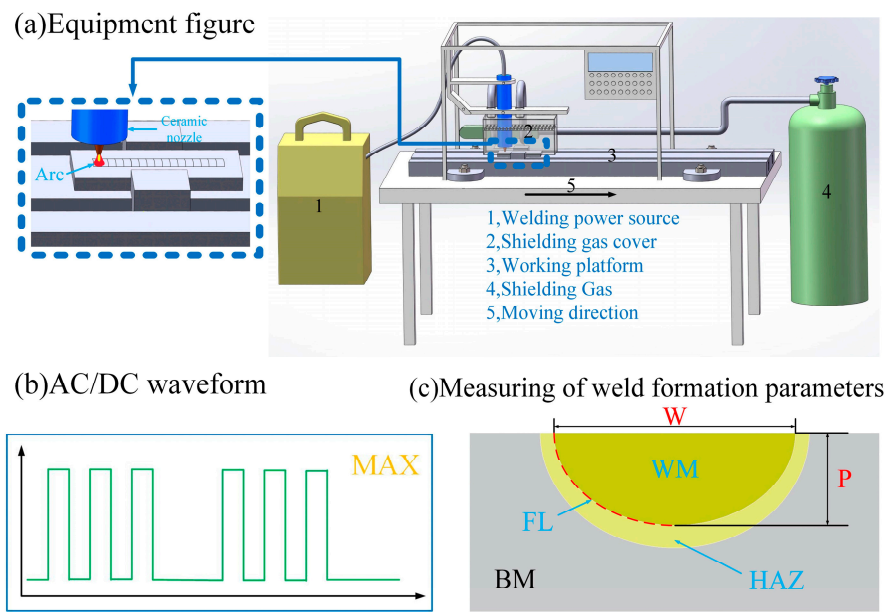


**Figure 1.** Schematic diagram of the experiment. (a) is equipment figure, (b) is AC/DC waveform, (c) is measuring of weld formation parameters.

**Table 2.** Experimental parameters of each group (%).

NO.	1	2	3	4	5	6	7	8	9	10	11
AC proportion	0	10	20	30	40	50	60	70	80	90	100

The surface of the base metal is polished by a polishing machine before welding in order to remove oxide film and grease. After the completion of welding, observe the weld forming surface and take photos to record it, as shown in Figure 2.

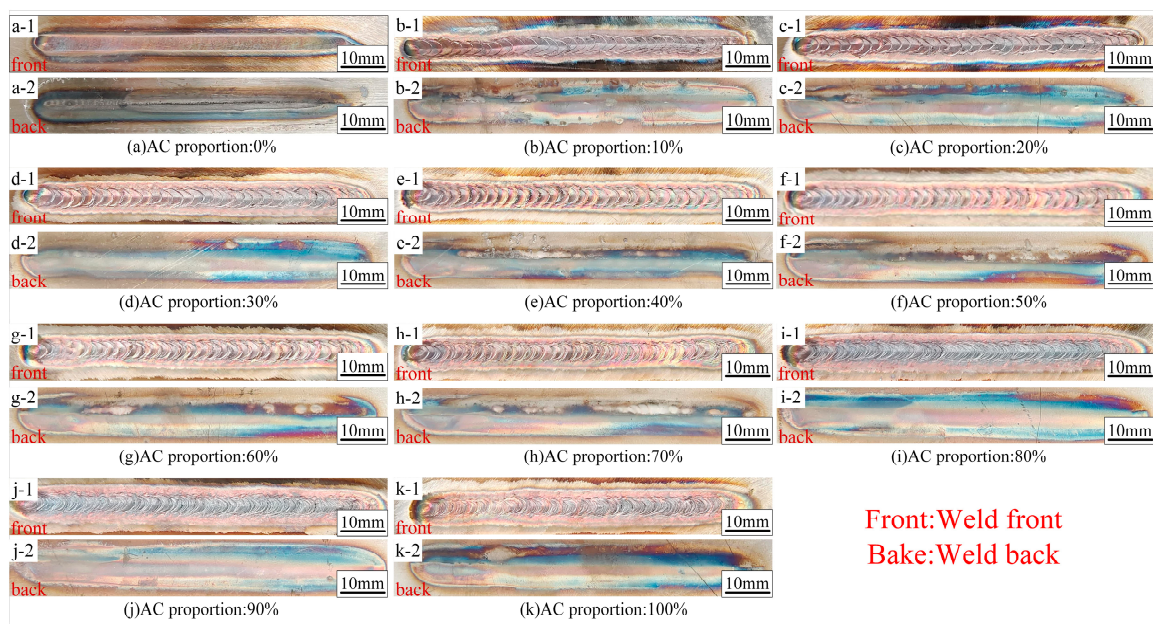


**Figure 2.** Appearance of weld forming. (a–k) correspond to a proportion of AC proportion from 0% to 100%, respectively.

The metallographic specimens are first inlaid and then coarsely ground and finely ground with 240 mesh, 400 mesh, 800 mesh, and 1200 mesh sandpaper. After the metallographic specimens are ground without visible scratches, they are polished on PG-1 metallographic sample polishing machine (Yongying Instrument, Ningbo, China.) and then corroded with corrosion solution. As soon as the metallographic specimens are corroded, they need to be quickly washed with distilled water to prevent excessive corrosion. The corrosion solution consists of 50 mL HCl, 10 mL HNO<sub>3</sub>, 100 mL H<sub>2</sub>O, and 10 g FeCl<sub>3</sub>. Finally, the weld tissue is observed with a light microscope.

Finally, the mechanical properties of the weld under different AC ratios are studied by a hardness test. The hardness test is conducted on an HVS—1000 microhardness tester (Shanghai Lian'er Testing Equipment Co., Ltd., Shanghai, China). The points in the hardness test are drilled through the weld along the welding width direction; the load is 500 g; the load holding time is 15 s, and the step length is 200  $\mu$ m.

### 3. Experimental Results and Discussion

#### 3.1. Weld Forming

##### 3.1.1. Weld Appearance

The bead-on-plate welds were made during TIG self-melting welding. Figure 2 is the appearance topography of 11 groups of welds in the experiment. The numbers 1 and 2 in the upper left corner of each weld picture represent the front and back of the weld, respectively. In DC mode, the surface is smooth and clean. Liu et al. found that each pulse current would form a point molten pool on the workpiece, and then the molten pool would be cooled during the base current, and finally a weld constructed by connecting multiple solder joints was obtained [12]. Additionally, in the welding of 304 stainless steel, the liquid metal on the surface of the molten pool flows from the edge of the molten pool to the center of the molten pool in a counterclockwise direction [10]. In the process of flow, the liquid metal gradually cools down, and the flow speed slows down. The thickness of the molten pool edge is larger than that of the molten pool center. The MIX mode in this experiment includes AC and DC, which change periodically. Therefore, in the AC and DC mixed mode, fish-scale lines appear in the weld, and each fish scale has thick edges and a thin middle. According to Figure 2, with the increase of the proportion of AC, the density of uniformly distributed fish scales increases. This is because with the increase of the proportion of AC, the frequency of AC changes increases; the formation time of fish scales is shortened, and fish scales are more densely distributed [11].

Compared with other cases, when the proportion of AC is 30–70%, the proportion of AC is larger; the overlap between solder joints is larger; the weld is more continuous, and the molding is more beautiful. Among them, when AC accounts for 50%, the welds have the most uniform distribution of fish scales, and the surface has the most beautiful metallic luster. When the proportion of AC is less than or equal to 20%, the overlap between solder joints is small and the weld pool is discontinuous. Therefore, the fish-scale pattern on the weld surface is not uniform, and the whole weld looks not straight enough. When the proportion of AC is greater than or equal to 80%, the density of fish-scale grain is too large, and the weld forming is relatively disordered. In welding, if there is more attention to beauty, it is recommended that AC account for about 50% [12].

##### 3.1.2. Weld Penetration and Weld Width and Their Ratio

The specimens' cross sections are shown in Figure 3. As shown in Figures 4 and 5, when AC accounts for 10%, the weld penetration, weld width, and the ratio of weld penetration to weld width are lower than those in DC mode. However, when the proportion of AC is greater than or equal to 20%, the weld penetration, weld width, and the ratio of weld penetration to weld width are higher than those in DC mode. MIX mode is overall higher than DC mode. The weld penetration, weld width, and the ratio of weld penetration to weld width increase and change in S-shape with the increase of AC proportion. Therefore, it is not that the larger the proportion of AC, the larger the melting width, and the larger

the ratio of melting depth to melting width. In the actual application of the project, it is necessary to select the appropriate AC proportion according to the specific requirements.

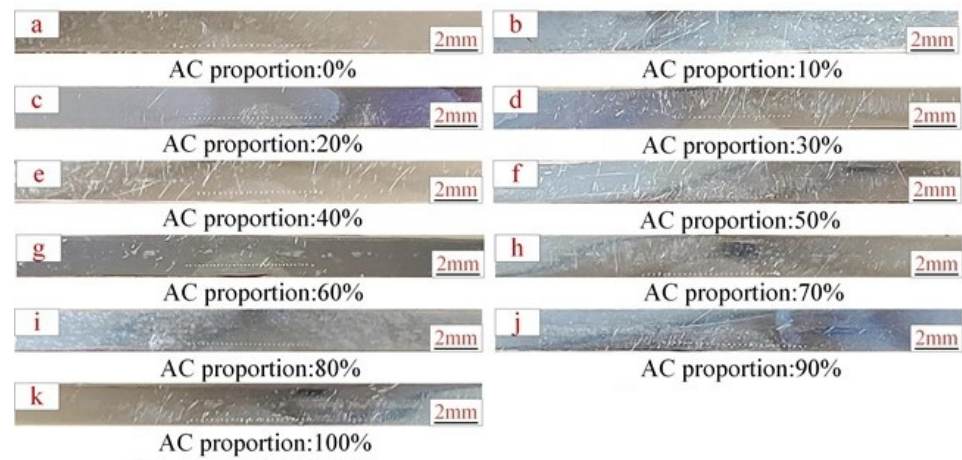


**Figure 3.** Specimens cross sections. (a–k) correspond to a proportion of AC proportion from 0% to 100%, respectively.

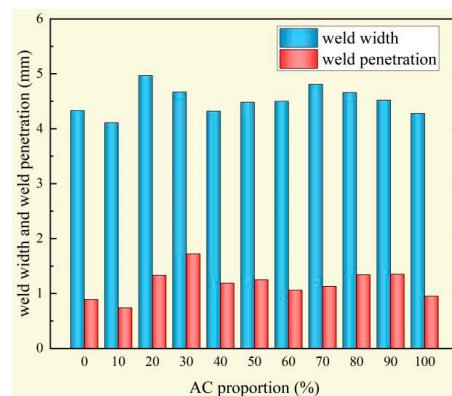


**Figure 4.** Weld penetration and weld width.

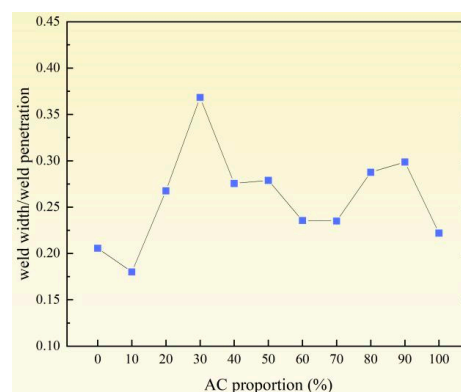


**Figure 5.** Ratio of weld penetration and weld width.

The experiment is statically processed, and the data for each group are measured five times, and errors are obtained. As shown in Table 3, the weld width of 20% AC is the largest, which is 4.97 mm, 0.64 mm larger than that of DC mode. Both weld penetration and the ratio of weld penetration to weld width are the highest when AC accounts for 30%. At this point, the weld penetration is 0.83 mm larger than DC mode, an increase of 93.26%, and the ratio of weld penetration to weld width is 1.6, which is 76.19% higher than DC

mode. When AC accounted for 10%, the weld penetration, weld width, and the ratio of weld penetration to weld width are all the minimum values in the experiment. The ratio of weld penetration to weld width is even 14.29% smaller than that of DC mode.

**Table 3.** Weld penetration and weld width.

AC Proportion	Weld Penetration (mm)	Weld Width (mm)	Weld Penetration/Weld Width
0%	$0.89 \pm 0.05$	$4.33 \pm 0.02$	$0.21 \pm 0.02$
10%	$0.74 \pm 0.02$	$4.11 \pm 0.03$	$0.18 \pm 0.01$
20%	$1.33 \pm 0.06$	$4.97 \pm 0.04$	$0.27 \pm 0.01$
30%	$1.72 \pm 0.01$	$4.67 \pm 0.04$	$0.37 \pm 0.01$

### 3.2. Microstructure

Eleven groups of weld microstructure are shown in Figure 6, which are composed of white austenite and black ferrite. When the welding current is DC, the microstructure of the weld is relatively disordered equiaxed crystal, and some appear columnar crystal when the proportion of AC increases. The columnar crystal is the weak zone of the weld, and the crack is easy to appear at the grain boundary. The columnar crystal grain boundary is the area with a high probability of bubbles, impurities, and shrinkage pores [26]. Yangyang Fan et al. showed that the grains in equiaxed zone crossed each other when they grew up and the lap between the forks was firm. Compared with columnar zone, crack propagation is difficult, and there is no obvious weak interface [27]. Therefore, equiaxed crystal has better performance than columnar crystal.

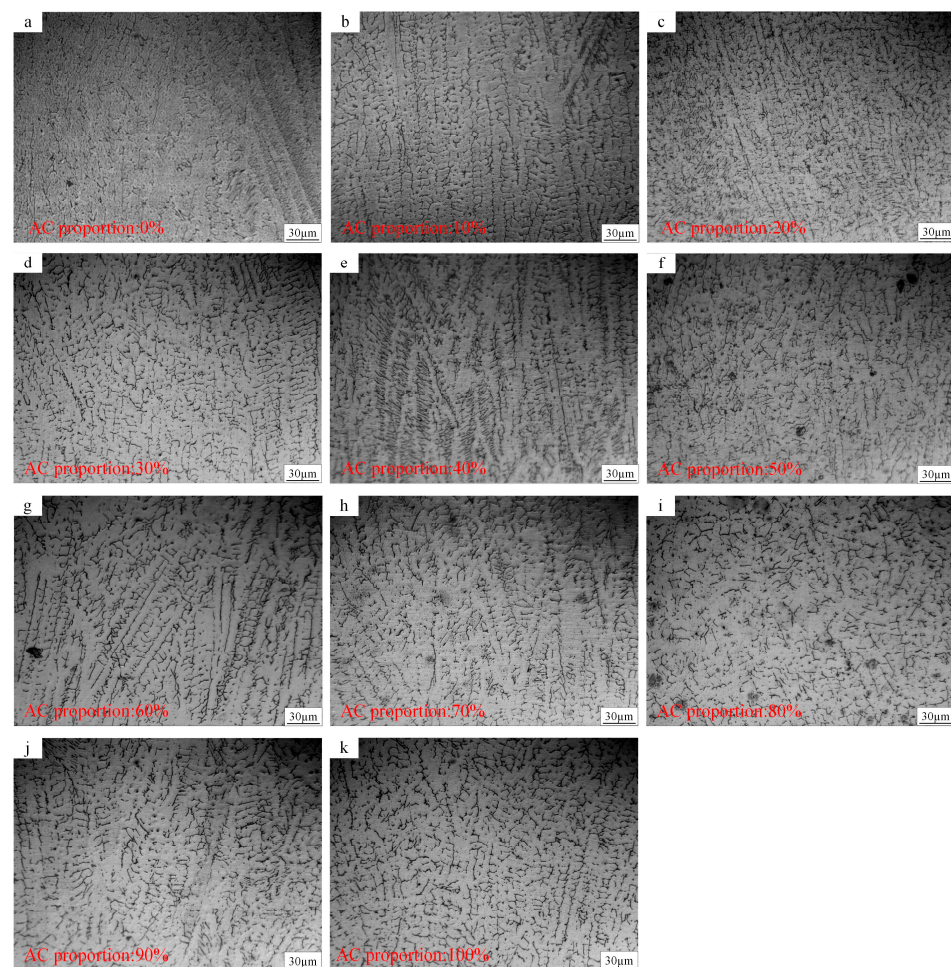


**Figure 6.** Weld microstructure. (a–k) correspond to a proportion of AC proportion from 0% to 100%, respectively.

When the AC ratio is 20% and 30%, the microstructure is transformed from columnar crystal with an AC ratio of 10% to equiaxed crystal. As can be seen from Figure 6, the ferrite grain is refined; the microstructure distribution is uniform, and the mechanical properties are optimal. When the proportion of AC is 40%, the crystal is obviously columnar. Although AC accounts for 50%, 80%, and 100% of equiaxed crystal, the grain size is larger than that of 20% and 30%, so the performance still cannot reach the optimum. When the proportion of AC is 70% and 90%, the microstructure is columnar crystal and some equiaxed crystal [28].

In Figure 7, the base metal (BM) is in the lower left corner of the picture; the heat affected zone (HAZ) is in the middle of the picture, and the weld (WM) is in the upper right corner. The junction between the heat affected zone and the weld is the fusion line. In the article of Bingbing Lu et al., the influencing factors of ferrite morphology include weld composition and cooling rate at different positions [29]. In this experiment, the base material is white austenite. In the process of cooling, the diffusion of ferrite into austenite is inhibited; the diffusion distance is reduced, and the ferrite appears as a lath form [30]. The weld is equiaxed or columnar due to the influence of temperature gradient. Reducing the width of heat affected zone can improve the performance after welding. The bar chart in the lower right corner of Figure 7 shows that the width of the heat affected zone is smaller than that of the DC width of the heat affected zone only when the AC ratio is 30%, 40%, and 60%. When AC accounts for 40% and 60%, the width is the smallest (77), which is 14.44% lower than that of DC. Therefore, not all the MIX mode have a smaller HAZ width than that in DC mode.

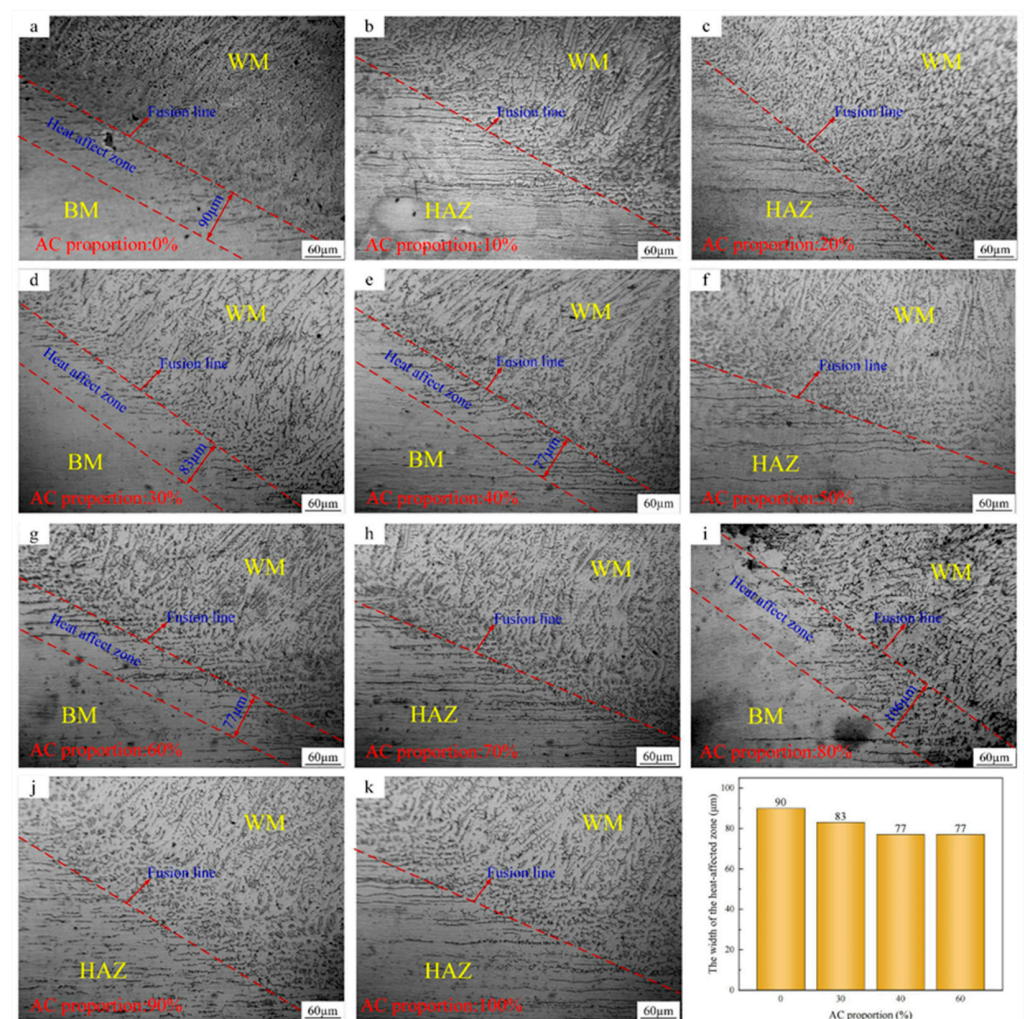


**Figure 7.** Metallographic microstructure. (a–k) correspond to a proportion of AC proportion from 0% to 100%, respectively, and the bottom right corner is a bar chart of the width of the heat affected zone.

### 3.3. Performance

#### Microhardness

Li Fei et al. showed that microhardness was an important index when judging the properties of materials, and the microstructure would affect the microhardness of materials [31]. The direction of hardness is a straight line along the weld width. Figure 8 shows the microhardness distribution of the base metal, heat affected zone, and weld under different AC proportions. As can be seen from Figure 8, the hardness of the heat affected zone is the lowest, and the average hardness of the weld is higher than that of the base metal. This is because the HEZ is composed of austenite and ferrite in lath form. Chen Yong et al. showed that microhardness can reflect the uniformity of internal tissues [30]. Therefore, when the proportion of AC is 50%, the size of the weld hardness is evenly distributed, and the average value is greater than the hardness of the base metal, indicating that the microstructure is relatively uniform.

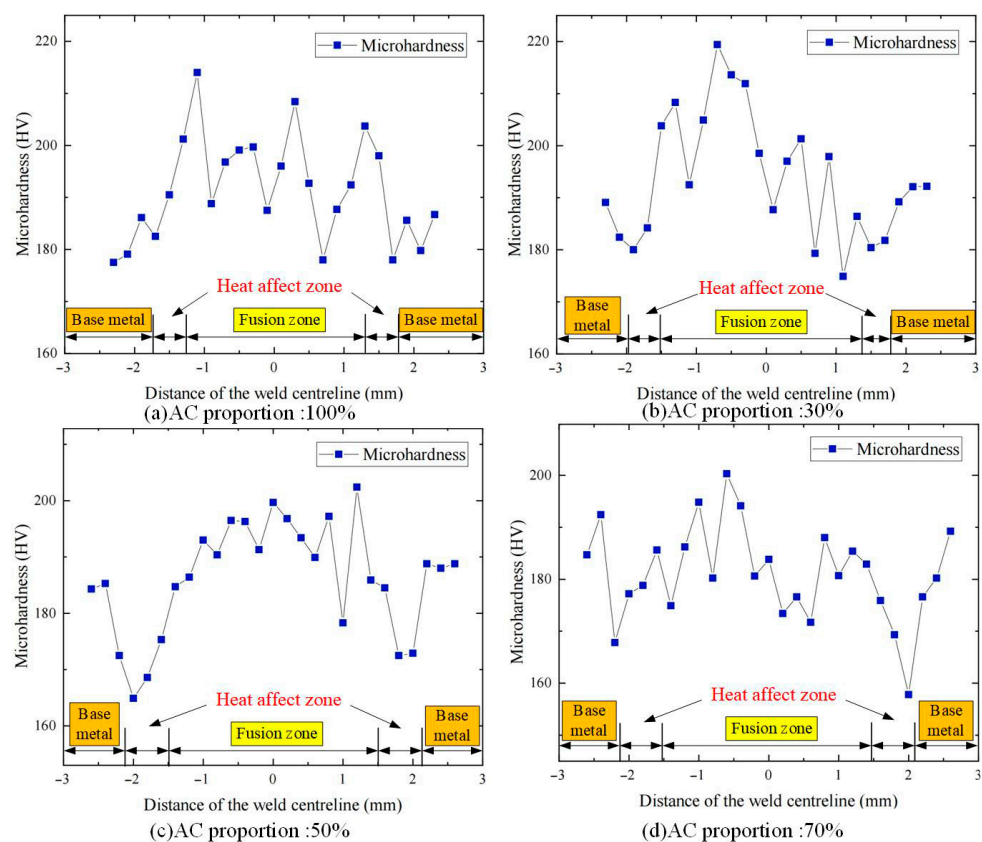


**Figure 8.** Microhardness distribution diagram. (a–d) are the distribution diagram of microhardness with AC proportion for 100%, 30%, 50% and 70%.

Figure 9 shows the bar chart of the average hardness of the weld under different AC proportions. When the proportion of AC is 20% and 30%, the average hardness values are 196.7 HV and 198.1 HV, respectively, which are 15.7 HV and 17.1 HV higher than the average hardness values in DC mode. This is because the weld microstructure is fine uniform equiaxed crystal, which has good mechanical properties. The average hardness of 60% AC is 179.6 HV, which is 1.4 HV lower than that in DC mode. This is because the weld microstructure is coarse columnar crystals. On the whole, the average weld hardness of MIX mode is greater than that of DC mode, and AC-DC mixing can improve the weld hardness.

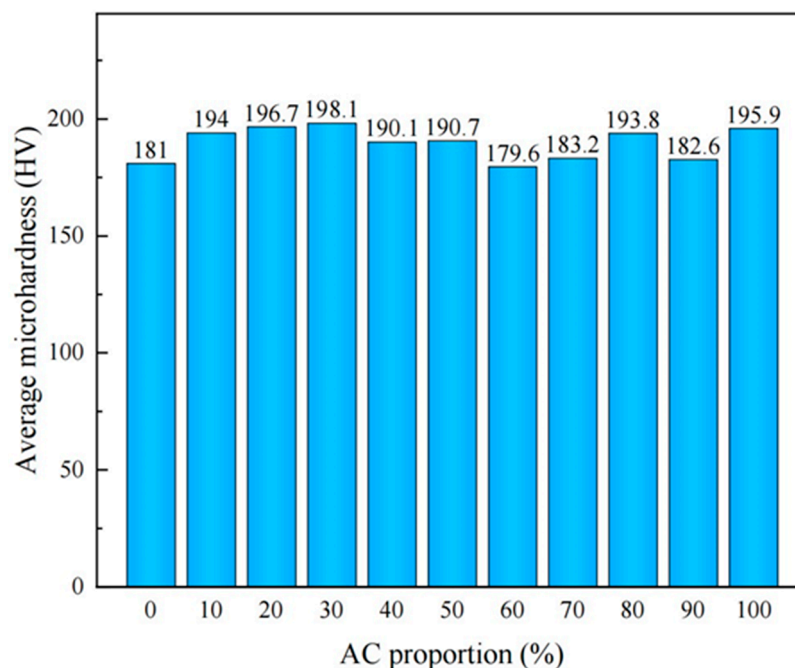


**Figure 9.** Bar chart of average weld hardness.

#### 4. Conclusions

- (1) The weld under AC/DC mixing is fish scale pattern, and the density of fish scale pattern increases with the increase of AC proportion. When the proportion of AC is 50%, the forming is the most beautiful; the surface has metallic luster, and the fish scales are evenly distributed.
- (2) When AC accounts for 10%, the weld penetration, weld width, and their ratios are smaller than those in DC mode. Both weld penetration and the ratio of weld penetration to weld width are the highest when AC accounts for 30%. At this point, the weld penetration is 0.83 mm larger than DC mode, an increase of 93.26%, and the ratio of weld penetration to weld width is 1.6, which is 76.19% higher than DC mode.
- (3) When the proportion of AC is increased, the microstructure of the weld is equiaxed or columnar, and the microstructure of the heat-affected zone is ferrite in the form of lath. The best performance is obtained when AC accounted for 20% and 30%, because the microstructure is fine and evenly distributed equiaxed crystal at this time. When the proportion of AC is too large, although the microstructure of weld is equiaxed, the grain size is coarse and the performance decreases.
- (4) The hardness of the weld is greater than that of the base metal, and the hardness of the heat-affected zone is the lowest. The microhardness distribution of the weld with AC 50% is the most uniform. The average hardness of welds with AC accounting for 20% and 30% is the largest, which are 196.7 HV and 198.1 HV, respectively.

**Author Contributions:** Conceptualization, X.Z. and Y.Y. (Ying Ye); methodology, X.Z.; software, B.Y.; validation, C.C., Y.Y. (Yonghui Yang) and Z.P.; formal analysis, Y.Y. (Ying Ye); investigation, Y.Y. (Ying Ye); resources, B.Y.; data curation, Y.Y. (Yonghui Yang); writing—original draft preparation, Y.Y. (Ying Ye); writing—review and editing, X.Z.; visualization, C.C.; supervision, X.Z.; project administration, X.Z.; funding acquisition, X.Z. All authors have read and agreed to the published version of the manuscript.

**Funding:** This work was financially supported by the Postdoctoral Science General Program of Heilongjiang Province [grant number: LBH-Z22045], the Fundamental Research Funds for the Central Universities through Grant [grant number: 2572021BF07], and the Fundamental Research Funds for the Central Universities through Grant [grant number: 2572022BF01].

**Data Availability Statement:** The data presented in this study are available in the article.

**Conflicts of Interest:** The authors declare no conflict of interest.

## References

1. Li, Y.; Fan, J.; Wen, J.; Nie, X.; Zhou, L. Study on the Effects of Multiple Laser Shock Peening Treatments on the Electrochemical Corrosion Performance of Welded 316L Stainless Steel Joints. *Metals* **2022**, *12*, 1215. [\[CrossRef\]](#)
2. Sarfarazi, S.; Shamass, R.; Mascolo, I.; Dellacorte, G.; Guarracino, F. Some Considerations on the Behavior of Bolted Stainless-Steel Beam-to-Column Connections: A Simplified Analytical Approach. *Metals* **2023**, *13*, 753. [\[CrossRef\]](#)
3. Yoo, Y.; Choi, S.; Kim, Y. Effect of Laser Shock Peening on the Stress Corrosion Cracking of 304L Stainless Steel. *Metals* **2023**, *13*, 516. [\[CrossRef\]](#)
4. Zhang, W.; Liu, F.; Liu, L.; Li, Q.; Liu, L.; Liu, F.; Huang, C. Effect of grain size and distribution on the corrosion behavior of Y<sub>2</sub>O<sub>3</sub> dispersion-strengthened 304 stainless steel. *Mater. Today Commun.* **2022**, *31*, 54. [\[CrossRef\]](#)
5. Xue, J.; Wu, H.; Zhou, C.; Zhang, Y.; He, M.; Yan, X.; Xie, H.; Yan, R.; Yin, Y. Effect of Heat Input on Hydrogen Embrittlement of TIG Welded 304 Austenitic Stainless Steel. *Metals* **2022**, *12*, 1943. [\[CrossRef\]](#)
6. Li, W.; Guo, T.; Xu, L.; Chen, L.; Jiang, B.; Wang, X.; Wu, H.; Qiao, L. Promotion of pitting corrosion at hydrogen-enriched phase boundaries in austenitic stainless steel weld joints. *Acta Mater.* **2022**, *227*, 117728. [\[CrossRef\]](#)
7. Zhou, C.; Liu, X.; Zhang, Y.; Wu, H.; Yang, Y. Numerical study on effect of inclusions on hydrogen segregation in steel under stress conditions. *Int. J. Hydrogen Energy* **2022**, *47*, 20310. [\[CrossRef\]](#)
8. Zhang, H.Y.; Hu, J.; Meng, X.M.; Sun, Y.; Wang, T.; Lv, W.J.; Shi, Q.X.; Ma, J.Y.; Zhou, D.Y.; Liang, W.; et al. Effect of deformation microstructures on hydrogen embrittlement sensitivity and failure mechanism of 304 austenitic stainless steel: The significant role of rolling temperature. *J. Mater. Res. Technol.* **2022**, *17*, 2831. [\[CrossRef\]](#)
9. Dong, Z.; Li, Y.; Wu, H.; Babkin, A.; Chang, Y. Effect of TIG arc characteristics on weld morphology and structure of AISI444 ferritic stainless steel under pulse current. *Weld. World* **2021**, *65*, 2093. [\[CrossRef\]](#)
10. Huang, J.; Sun, T.; Ding, F.; Yu, S. Study on the Surface Flow Behavior of TIG Weld Pool. *J. Mech. Eng.* **2016**, *18*, 31. [\[CrossRef\]](#)
11. Ramkumar, K.; Chandrasekhar, A.; Srivastava, A.; Preyas, H.; Chandra, S.; Dev, S.; Arivazhagan, N. Effects of filler metals on the segregation, mechanical properties and hot corrosion behaviour of pulsed current gas tungsten arc welded super-austenitic stainless steel. *J. Manuf. Process.* **2016**, *24*, 46. [\[CrossRef\]](#)
12. Liu, T.; Chen, H. Influence of Pulse TIG Welding Process Parameters on Weld Forming of Sheet Stainless Steel. *Hot Work. Technol.* **2015**, *44*, 187.
13. Nima, N.; Majid, P. Transition in Interfacial Failure Mechanism of Resistance Spot Welds during Tensile–Shear Loading: Role of Fusion Zone Hardness. *Metals* **2023**, *13*, 1076.
14. Francisco, B.; Igor, F.; Isaque, B.; João, P.; Telmo, S. A Review of Orbital Friction Stir Welding. *Metals* **2023**, *13*, 1055.
15. Singh, A.; Dey, V.; Rai, R. Techniques to improve weld penetration in TIG welding (A review). *Mater. Today Proc.* **2017**, *4*, 1252. [\[CrossRef\]](#)
16. Li, C.; Liu, L. Investigation on weldability of magnesium alloy thin sheet T-joints: Arc welding, laser welding, and laser-arc hybrid welding. *Int. J. Adv. Manuf. Technol.* **2013**, *65*, 27. [\[CrossRef\]](#)
17. Xie, W.; Fan, C.; Yang, C.; Sanbao, L. Influences of acoustic field parameters on welding arc behavior in ultrasonic-MIG welding. *China Weld. Engl. Ed.* **2015**, *24*, 29.
18. Wang, Y.; Qi, B.; Cong, B.; Yang, M. Optimization of hybrid ultrasonic frequency pulsed VP-GTAW process parameters on tensile properties of AA 5456 Alloy. *Appl. Sci.* **2017**, *7*, 48. [\[CrossRef\]](#)
19. Cong, B.; Qi, B.; Zhou, X.; Luo, J. Effect of Superaudio Pulse Square Wave Current Parameters on Weld Microstructure and Mechanical Properties of 2219 Aluminum Alloy. *Acta Metall. Sin.* **2009**, *45*, 1057.
20. Sharifitabar, M. Microstructure and mechanical properties of resistance upset butt welded 304 austenitic stainless steel joints. *Mater. Des.* **2011**, *32*, 3854. [\[CrossRef\]](#)
21. Gui, X.; Zhang, Y.; You, D.; Gao, X. Numerical simulation and test for influence of laser arc hybrid welding sequence on 304 stainless steel T-joint. *Trans. China Weld. Inst.* **2021**, *12*, 34.
22. Lee, J.K. Nondestructive Evaluation on Hydrogen Effect of TIG Welded Stainless Steel for Component Design of Pressure Vessel. *J. Power Syst. Eng.* **2017**, *3*, 102.
23. Yang, M.; Yang, Z.; Qi, B. Effect of fluid in molten pool on the welds with Ti-6Al-4V during pulsed arc welding. *Int. J. Adv. Manuf. Technol.* **2015**, *5*, 1007. [\[CrossRef\]](#)
24. Wang, Y.; Chen, M.; Wu, C. High-frequency pulse-modulated square wave AC TIG welding of AA6061-T6 aluminum alloy. *Weld. World* **2020**, *10*, 1749. [\[CrossRef\]](#)
25. Manti, R.; Dwivedi, D. Microstructure of Al-Mg-Si weld joints produced by pulse TIG welding. *Mater. Manuf. Process.* **2007**, *1*, 57. [\[CrossRef\]](#)
26. Cui, Z.; Liu, B. *Metallogry and Principle of Heat Treatment*; Harbin Institute of Technology Press: Harbin, China, 1998; p. 51.
27. Fan, Y.; Sun, Q.; Yang, C.; Liu, S.; Fan, C. TIG welding of the stainless steel 304 based on the ultrasonic vibration. *Trans. China Weld. Inst.* **2019**, *30*, 91.
28. Cao, Z.; Wu, D.; Su, H. Influence of External Magnetic Field on Microstructure and Properties of Stainless Steel TIG Welding Joint. *Hot Work. Eng.* **2009**, *38*, 134.
29. Lu, B. Study on Laser Welding Process of 304 Stainless Steel Sheet. *Hot Work. Work. Arts* **2023**, *52*, 145.

30. Chen, Y.; Lu, J.; Xu, L.; Wang, Y.; Zhang, T. Study on Microstructure and mechanical properties of Longitudinal Joints of 304 Stainless Steel Thin Wall Pipe Fitting under Different Welding Processes. *Hot Work. Ski.* **2022**, *51*, 127.
31. Li, F. Microstructure and Performance Analysis of Ultrasonic assisted CMT Welded Joint of 304 Stainless Steel. *Inn. Mong. Ind. Learn.* **2021**, *11*, 71.

**Disclaimer/Publisher's Note:** The statements, opinions and data contained in all publications are solely those of the individual author(s) and contributor(s) and not of MDPI and/or the editor(s). MDPI and/or the editor(s) disclaim responsibility for any injury to people or property resulting from any ideas, methods, instructions or products referred to in the content.